

# Machine learning backpropagation network analysis of permeability, Forchheimer coefficient, and effective thermal conductivity of macroporous foam–fluid systems



Abdulrazak Jinadu Otaru<sup>a,\*</sup>, Manase Auta<sup>b</sup>

<sup>a</sup> Chemical Engineering Department, King Faisal University, P.O. Box 380, Al-Ahsa, 31982, Saudi Arabia

<sup>b</sup> Department of Chemical Engineering, Federal University of Technology, P.M.B. 065, Gidan-Kwau Campus, Minna, Nigeria

## ARTICLE INFO

### Keywords:

Macroporous structures  
Machine learning  
Permeability  
Forchheimer coefficient  
Effective thermal conductivity

## ABSTRACT

Macroporous materials exhibit outstanding properties in heat and mass transfer due to their high pore volume, high surface area, and high Young's modulus. Consequently, understanding their thermofluidic properties is crucial in the design, synthesis, and optimal application of these materials. Therefore, this study, premieres, the use of a machine learning (ML) backpropagation network to develop and train a series of datasets for permeability, Forchheimer coefficient, and effective thermal conductivity of variable macroporous foam–fluid systems with respect to degrees of interstices, fluid and solid properties. To account for permeability values for flowing fluids in the Darcy regime, numerical simulations of slow-moving fluids were implemented over the materials' interstices. In comparison to similarly substantiated values of permeability in the Forchheimer regime, these values were a bit lower. The ML-based backpropagation algorithm was used to analyze data, which produced predictions (output signals) that are more than 90 % in correlation to CFD datasets. This provided insight into the effect of porosity and reduced mean pore openings on macroporous structures' thermofluidic behaviour. Material porosity was observed to play a dominant role in estimating Forchheimer coefficients and effective thermal conductivities for these foam–fluid systems. However, reduced mean pore openings were observed to be more critical for estimating permeability. The contributory effects of reduced mean pore openings on the effective thermal conductivity for these macroporous foam–fluid systems were determined to vary between 5.8 and 13.2 percent. Furthermore, the effective thermal conductivity of macroporous foam–fluid systems was also evaluated in relation to changes in the interstitial fluid and solid matrix thermal conductivity.

## 1. Introduction

Porous media fluid transport has been studied for well over fifteen decades, beginning with Henry Darcy's 1856 article [1] on groundwater flow in granular/aggregate media. The majority of these studies have focused on fluid transport in porous media that naturally occur, namely packed structures and granular materials [2–7], which are known for their low porosity (typically 0.33 for densely packed structures and 0.6 for loosely packed structures [8]) and increased surface area and pressure drop due to their increased surface wettability [8–10]. Specifically, this study focuses on macroporous structures with high pore volume fractions (porosity) and surface area in comparison with granular materials [10]. Currently, there are relatively few articles published on macroporous structures compared with those for granular or packed

structures.

Macroporous materials, usually made from metals, are lightweight constructs containing randomly distributed pores and interconnected pore openings or connectivity [11]. They are classified as either open-celled foams [12,13] or closed-celled foams based on their interconnected network, which provides tortuous flow within the interstices. Fig. 1 presents images of sponge-like (Fig. 1a) and bottleneck-shaped (Fig. 1b) porous metallic materials. While Fig. 1a illustrates a highly open structure characterized by ligaments, typified by dodecahedron-like cells with 12–14 pentagonal or hexagonal faces [14], Fig. 1b is characterized by low porosity, larger and near-circular pores, and smaller openings [15,16]. Boomsma et al. [17] noted that the large contact area per unit volume (ranging between 500 and 3,000 m<sup>2</sup> m<sup>-3</sup>) provided by the internal pores in porous metallic structures allows for

\* Corresponding author. Chemical Engineering Department, King Faisal University, P.O. Box 380, Al-Ahsa, 31982, Saudi Arabia.

E-mail addresses: [aotaru@kfu.edu.sa](mailto:aotaru@kfu.edu.sa), [otaru\\_12257@yahoo.com](mailto:otaru_12257@yahoo.com) (A.J. Otaru).

fluid mixing, resulting in enhanced heat transfer which is significantly influenced by the ligament or solid content within the metal matrix. With their high porosity, sufficient surface area, high Young modulus, and thermal stability, metal foams are amongst the most recently studied materials utilized in many heat and mass transport systems. A few examples of these applications include petroleum reservoirs, condensers, catalyst supports, high-power batteries, sound absorbers, multifunctional heat exchangers, automobile catalytic converters, filtration, reactors, fuel cells etc. [16–20].

Heat and mass transfer through macroporous structures requires a comprehensive understanding of velocity and pressure disposition across their interstices at low and high velocities. In addition, it requires an understanding of how temperature changes across the material. When fluid velocities are very low or creeping, the permeability ( $k_0$ ) of porous materials are considered important, but at high fluid velocities, the Inertial or Forchheimer coefficient dominates porous media flow [21–24] – which can be mathematically expressed using equation (1) of the Darcy-Dupuit-Forchheimer model.

$$\frac{\Delta P}{L} = \frac{\mu}{k_0} u_s + \rho \frac{C_F}{k_0} u_s^2 \text{ and } C = \frac{C_F}{k_0} \quad \text{Eqn 1}$$

$$\frac{\Delta P}{L} = \frac{\mu}{k_0} u_s \text{ [Darcy flow]} \quad \text{Eqn 2}$$

where  $\Delta P/L$  is the unit pressure drop,  $\mu$  is the fluid dynamic viscosity,  $\rho$  is the fluid density,  $C_F$  is the Forchheimer coefficient, and  $u_s$  is the superficial fluid velocity. Similarly, the effective thermal conductivity ( $k_{eff}$ ) of the foam–fluid system is used to describe the effect of interstitial fluid and solid matrix heat conductivity [17–20,25].

Previously, researchers have employed experimental, analytical, and numerical methods to determine the permeability, the Forchheimer coefficient, and the effective thermal conductivity of macroporous structures in published articles on fluid and thermal transport in macroporous structures. For instance, studies conducted by Paek et al. [12] and Liu et al. [10] used experimental measurements of pressure drop versus superficial fluid velocity to determine the permeability and Forchheimer coefficient of metal foams by fitting the data to Eqn (1). According to Paek et al. [12], pressure drop data for metal foams were inconsistent, while those for packed beds were evidently consistent. Liu et al. [10] concluded that the pressure drop in metal foams is one-eighth that of granular materials due to increased surface wettability of the latter. Bhattacharya et al. [2] used air and water as the interstitial fluid media to determine aluminum and reticulated vitreous carbon (RVC) foams' effective thermal conductivity ( $k_{eff}$ ), permeability ( $k_0$ ), and Forchheimer coefficient ( $C_F$ ). They found permeability and the Forchheimer coefficient to be dominant at very low and high velocities, respectively, in these porous media. The Forchheimer coefficient was observed to be inversely proportional to foam porosity while permeability increased with foam porosity and pore diameter. Using high porosity metal foams in the post-Darcy regime, Bağci & Dukhan [26]

explored the effects of pore density on their hydrodynamics. While the foams had somewhat similar porosities (typically, between 87.6 and 88.5 percent), their permeability and Forchheimer coefficients significantly deviated from one another, where the pore size of the materials was noted to play only a minor role in regime transition.

Furthermore, the effective thermal conductivity of the materials was observed to be linearly inverse to the material's porosity and was observed to be strongly influenced by the thermal conductivity of the solid ligaments over the interstitial fluids within the pores. The combined use of X-ray computed tomography datasets and three-dimensional imaging in Refs. [15,27] revealed the importance of pore-structure-related and flow information on tetrakaidekahedron [27] and bottleneck-shaped porous metallic foams [15]. In their work, numerical simulations of pressure drop data (Fig. 1) showed that permeability and form drag increased and/or decreased with increasing material porosity, respectively. In separate studies working from X-ray computed tomography datasets [28] and sphere-packing models [29], the effective thermal conductivity of bottleneck-shaped macroporous structures were obtained, and compared with experimental values for similar foam materials presented in Refs. [30,31], as seen in Fig. 2c. They differed from those in Refs. [25,32] due to differences in their porous morphology and their porosity. Although Calmudi & Mahajan [25] reported earlier a linear inverse relationship between effective thermal conductivity and porosity (ranging between 0.90 and 0.98) of aluminum foams. Based on an idealized three-dimensional (3D) cell geometry of tetrakaidecahedron (TKD) foam with a porosity ( $\epsilon$ ) of 0.95, a theoretical model for the thermal conductivity of both air- and water-saturated foam-fluid systems was developed in Ref. [33]. Water saturation was noted to contribute significantly to the overall effective thermal conductivity of the foam-fluid system over air saturation, with the conductivity of the solid content within the metal matrix also contributing significantly to the  $k_{eff}$  of the material. According to Dai et al. [34], the analytical determination of the foam ligament orientation was considered inconsistent in Ref. [32], and a reviser published in Ref. [35] to correct these errors. An experimental and computational fluid dynamics (CFD) modelling and simulation approach was used in Refs. [28–31] to determine the effective thermal conductivity of low porosity (ranges between 0.55 and 0.80) metal foams. As well as having an inverse relationship with porosity (see Fig. 2c), only small changes in  $k_{eff}$  are seen with mean pore diameter and openings.

Artificial intelligence techniques are currently being employed to develop a better understanding of porous metallic foams' heat and mass transport properties. For example, Tikadar & Kumar [36] used five different machine learning based regression models to predict and optimize the thermal-hydraulic performance of metal foam heat sink with reasonable correlations between experimental and predicted outputs. The best correlations were found with artificial neural networks (ANNs) and support vector regression techniques of the ML-based models, with mean absolute percent errors of less than 3.1%. A large set of experimental data points were collected, developed, trained and validated with an ANN model in Ref. [37]. Accordingly, ANN models

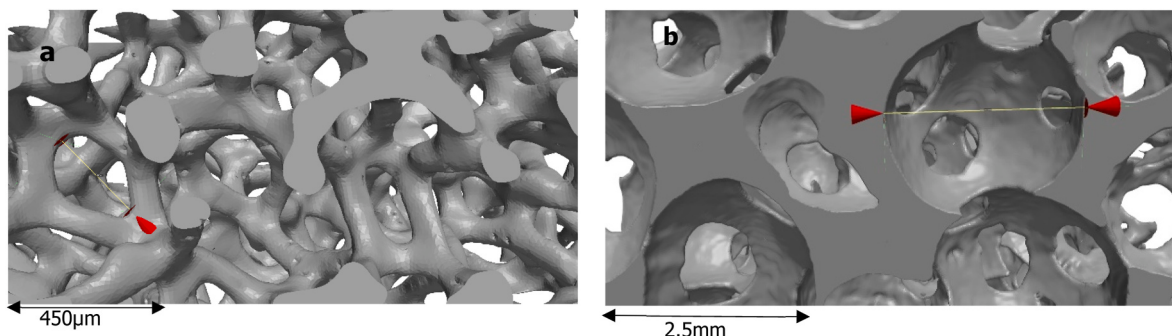


**Fig. 1.** Images of Inconel 450 µm (a) and aluminium foam structures (b) showing typical pore network, size and pore openings.

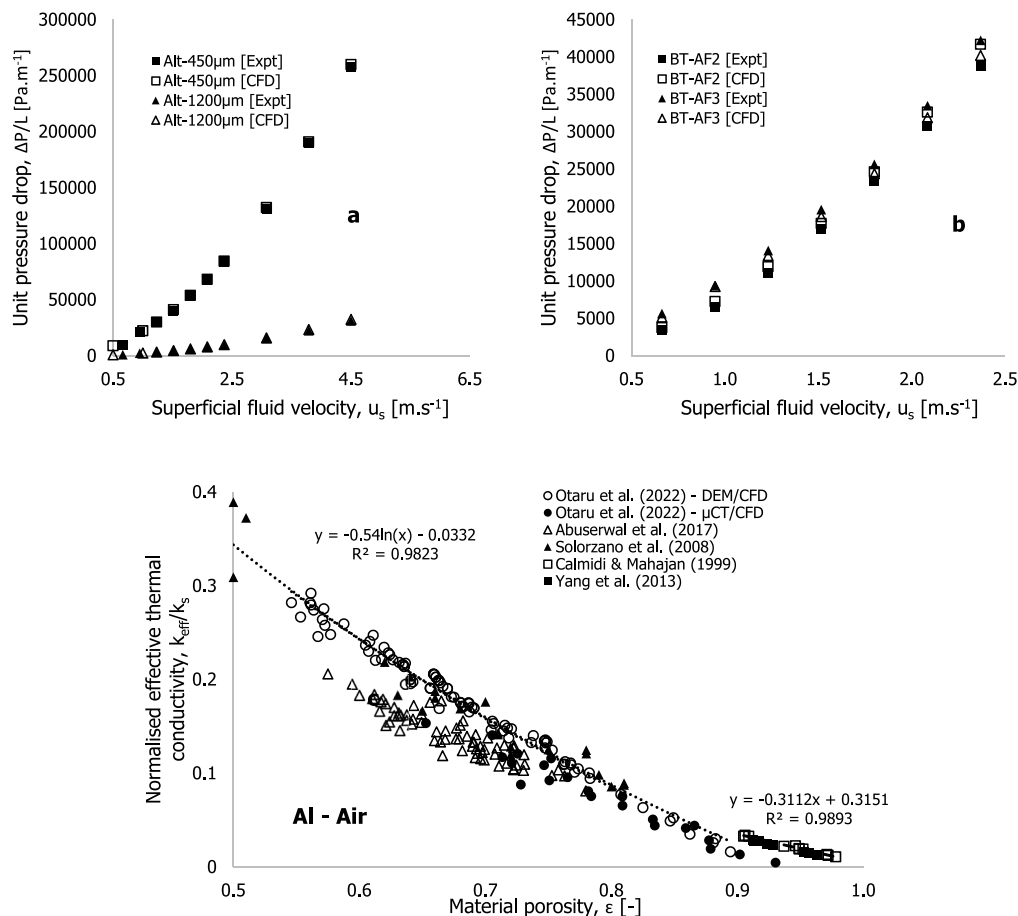


**Fig. 2.** Plots of experimentally measured and CFD modelled data of unit pressure drop,  $\Delta P/L$  [Pa.m<sup>-1</sup>] against superficial fluid velocity,  $u_s$  [m.s<sup>-1</sup>] for (a) Alantum 450 & 1200  $\mu$ m [27] (b) Bottleneck-shaped aluminium foam samples [14] and (c) plots of measured [25,30–32] and numerically computed [28,29] normalised effective thermal conductivity,  $k_{eff}/k_s$  [-] against material porosity for different class of macroporous structures.

were adjudged to successfully predict the intrinsic complexity of water pools boiling in metal foams as they deviated by less than 10 percent from experimental variance. An adaptive network-based fuzzy inference system (ANFIS) was used by Babanezhad et al. [38] to predict the hydrodynamic behaviour of heat transfer in metal foams under constant heat flux, where reasonable correlation with experimental work was obtained.

There have been several experiments and predictions made about the heat and mass transport in porous metallic foams, but little is known about using machine learning to analyze macroporous foam–fluid systems for thermofluidic properties and quantified the effects of pore-structure-related parameters, fluid, and structure on their thermofluidic performance. Additionally, discrepancies between different studies on heat and mass transport in porous metallic materials has somewhat adversely affected their application. This work, therefore, for the first time, uses machine learning backpropagation network analysis of an artificial neural networks (ANN) to develop, train, and predict the permeability ( $k_0$ ), the inertial Forchheimer coefficient ( $C_F$ ) and the effective thermal conductivity ( $k_{eff}$ ) of macroporous foam – fluid systems with pore volume fractions between 0.57 and 0.93.

## 2. Research approach

The approach used in this study can be divided into three categories:

1. Collection, development, and training of permeability ( $k_0$ ) and Forchheimer coefficient ( $C_F$ ) data for both “real” and “semi-virtual

structural-eroded” tetrakaidekahedron-shaped (Alantum 450  $\mu$ m, Alantum 1200  $\mu$ m) and bottleneck-shaped aluminium (BT-AF) foams produced using the inverse-replication casting technique described in Refs. [11,15,16]. These materials have a cylindrical shape, measuring 21.13 mm in diameter and 20 mm in height.

2. Collection, development, and training of porosity and effective thermal conductivity data for macroporous materials described in Refs. [28,29].
3. Values of  $k_0$  and  $C_F$  in step 1 were computed at Forchheimer regime for airflow across the interstices. Consequently, three-dimensional imaging and characterization of foam samples would be necessary to determine their permeability at Darcy regimes.

A detailed description is provided below for the third approach. It is important to note that the approach used in this section is called pore-level numerical simulation. Lorreyte et al. [39] showed that pore-level modelling is preferable to simple models of porous media for determining the transport properties of oak–wood chips because they contain anisotropic solid phases and have complex morphologies. The use of this approach has been successful in similar research on the transport properties of porous materials [15,22,28]. This study utilized a Zeiss Xradia Versa XRM-500 X-ray computed tomography system to acquire 2D high-resolution data sets (26  $\mu$ m voxel size) of porous metallic samples. These data were then processed, filtered and segmented with the ScanIP module of Synopsys-Simpleware™ (a 3D advanced imaging and characterization software), as TIFF files. Three-dimensional (3D) representative volume elements (RVE) were determined by shrinking

larger volumes into smaller cubic or rectangular-shaped structures until their porosity differed by  $\pm 3$  percent from that of the “real” materials. The nominal porosity of the “real” material was measured using a mass scale with a known value of density from the manufacturer’s datasheet (see Table 1, to be discussed later). Semi-virtual structures resembling “real” samples were created by erosion (pixel removal) of the “real” RVE [15,16]. Using this method consistently generates several “semi-virtual” samples, which increases the porosity of the original samples to near unity (i.e.  $\epsilon \leq 0.93$ ), as well as pore size and the mean pore opening of the materials at the same time. The ScanIP was used to measure pore structure related parameters (porosity, tortuosity, volume, mean pore size, mean pore openings, and specific surface) of the RVE structures. Tortuosity was calculated as a ratio of Euclidean to boundary distances, while specific surface was computed as a ratio of surface area of the solid content to bulk volume. A watershed segmentation of Boolean-inverted solid matrix was used to determine the mean pore size of the structure, and a centreline statistic was used to determine the mean pore opening of macroporous structures.

An analysis of the RVE fluid volume was conducted via meshing and mesh-dependent analysis in order to determine the gradient of velocity, capable of fast convergence and accuracy. The mesh dependence study started with a hexahedral quadratic tetrahedral mesh structure on one of the bottleneck-shaped RVE fluid domains, resulting in a maximum edge length of 15  $\mu\text{m}$  and a mesh density of 26 MCells. This mesh structure took an average of 6 h to compute individual flow information on a 64 GB RAM supercomputer. Nevertheless, the study resulted in a comparison of linear tetrahedral mesh structures with well-optimized linear structures that captured the gradient of velocity across macroporous structure’s interstices. Therefore, linear tetrahedral mesh (LTM) densities ranging from 2.5 to 3.5 MCells, a 1.3 growth rate, and edge lengths of 65 and 182  $\mu\text{m}$  were found to be feasible for all foam structures considered herein. COMSOL Multiphysics 5.2TM’s CFD module was used to solve Stoke’s equation by setting the inlet, outlet, and lateral faces to velocity, zero pressure, and symmetrical boundaries, respectively. Numerical representation of fluid physics was done with a multigrid solver, taking approximately 10–30 min per sample for creeping flow velocity (0–0.03  $\text{m s}^{-1}$ ). This velocity range was determined using the concept of pore-diameter-based Reynolds number ( $R_{eD} \leq 1.0$ ) for fluid flow in porous media within the Darcy or creeping region, described in Refs. [9,44,45]. Numerically simulated data on pressure drop across the material(s) were divided by their unidirectional flow thickness to determine the unit pressure drop per unit length. The pressure-velocity data was then fitted into the Darcy equation (Eqn (2)) to determine the permeability of the structures. It is noteworthy to mention that while flow data obtained for these structures was reportedly [15] conducted only on the RVE fluid domain, a numerical determination of the  $k_{eff}$  of these materials has been conducted previously [28,29] for a foam-fluid system, with reasonable correlation between experimental variance and modelled data as shown by Figs. 1 and 2.

**Table 1**  
Pore-structure-related and Darcian permeability data for all the “real” foam samples.

Foam type	Mean Pore Sizes, $D_p$ [mm]	Mean Openings, $D_w$ [mm]	Porosity ( $\epsilon$ )	Specific Surface, $\sigma_{FB}$ [ $\text{mm}^{-1}$ ]	Tortuosity [-]	Permeability $k_D/10^{-09}$ [ $\text{m}^2$ ] Darcy
Alt-450 $\mu\text{m}$	0.45	0.24	0.84	8.63	1.520	1.24 1.59 [ref 40]
Alt-1200 $\mu\text{m}$	1.23	0.49	0.91	3.22	1.380	15.56 21.00 [ref 41]
BT-AF1	2.23	0.69	0.71	2.65	1.71	11.10 3.50 [ref 15]
BT-AF2	2.22	0.72	0.73	2.52	1.68	13.90 17.10 [ref 15]
BT-AF3	0.77	0.24	0.73	4.59	1.67	3.91 4.09 [ref 42]
BT-AF4	2.77	0.71	0.75	2.25	1.65	20.40 18.98 [ref 43]

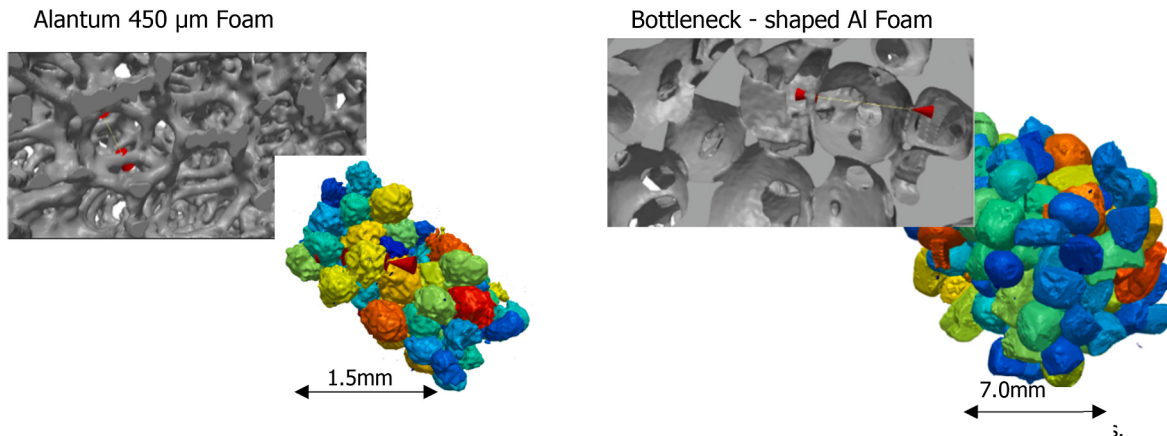
NB: Below the simulated data are related literature values for permeability substantiated in the literature.

### 3. Pore-structure-related and CFD computed flow data

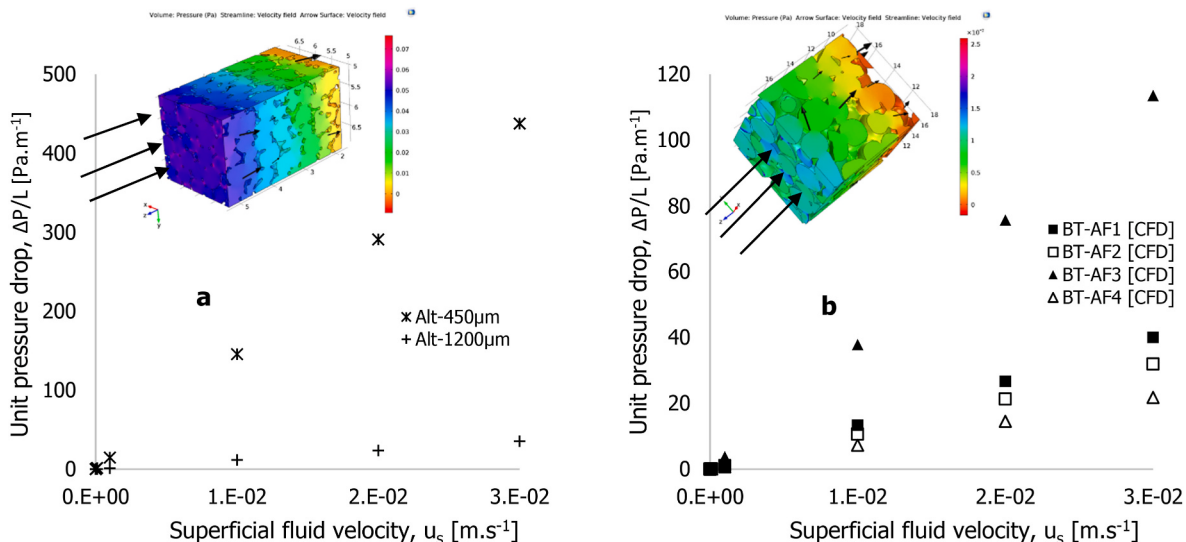
Fig. 3 illustrates typical morphological features of Alantum 450  $\mu\text{m}$  (left) and aluminium foam (right) along with their segmented pores. Optical and X-ray CT images of these materials reveal that both the Alantum samples used in this study are characterized by tetrakaidecahedron-shaped (TKD) pores linked by a mean ligament thicknesses of 59 and 176  $\mu\text{m}$  respectively. A bottleneck-shaped pattern was observed for the aluminium foam samples (BT-AF) which were produced by replication-casting techniques. In addition, some of the pores within the aluminium foams are not entirely spherical which may be related to the non-homogeneity of the salts used during the casting process (i.e. presence of half-sized salts). A detailed description of this process is given in Refs. [15,42].

Fig. 4 shows plots of TKD and BT-AF foams’ unit pressure drop vs. superficial fluid velocity (0–0.03  $\text{m s}^{-1}$ ). The three-dimensional RVE streamline/arrow plots in this figure demonstrate fluid flow in directions of pressure gradients where pressure decreases from inlet to exit for the structures. A linear relationship was also found between pressure and velocity for this creeping flow. The reason for this may be that fluid flow at slow velocities in porous media is largely determined by topology as fluid viscosity plays a crucial role in estimating the pressure drop developed across interstices [11,21,44]. Both the Alantum 450  $\mu\text{m}$  and BT-AF3 foams achieved higher unit pressure drops across their interstices—being materials with extremely low values of mean pore openings, as shown in Table 1. All metal matrices exhibited the same characteristics, with developed pressure drop inversely related to mean pore openings. Therefore, changes in the mean pore openings of porous metals have a substantial impact on flow behaviour. Furthermore, Table 1 shows that porosity and tortuosity are inversely related. For example, sample BT-AF1 with the lowest porosity value of 0.69 had the highest tortuosity value (1.71), while the Alantum 1200  $\mu\text{m}$  foam sample with the highest porosity value of 0.91 had the lowest tortuosity value (1.38). More so, materials with the lowest mean pore size (Alt-450  $\mu\text{m}$ ) exhibited the highest value of specific surface ( $8.63 \text{ mm}^{-1}$ ) – indicating a higher level of solid content in metal matrixes (responsible for restricting flow passage) compared to structures with a large mean pore size.

Table 1 also shows that the Darcy regime values of computed permeability ( $k_D$ ) increase with increasing value of mean pore openings of the materials. In comparison with published literature, most foam samples had lower permeability than similar metallic materials for inertial-dominated flows ( $k_i$ ). All samples had ratios between the two regimes of permeability (i.e.  $k_i/k_D$ ) that ranged between 0.93 and 1.35, which is consistent with the values of 1.02–1.52 established in Ref. [16] for mid to high porosity metal foams. According to Ref. [16], this low permeability is due to the solid content of the material, which resists slow-moving fluids. Flowing fluid reportedly permeates more interstitial pores within the solid matrix at high superficial velocity [16], enhancing the contact between moving fluid and pore walls, leading to



**Fig. 3.** Photographic and 3D processed images of Alantum 450  $\mu\text{m}$  and Bottleneck-shaped aluminium foam structures.



**Fig. 4.** Plots of CFD modelled unit pressure drop,  $\Delta P/L$  [ $\text{Pa} \cdot \text{m}^{-1}$ ] against superficial fluid velocity,  $u_s$  [ $\text{m} \cdot \text{s}^{-1}$ ] for (a) Alantum 450 & 1200  $\mu\text{m}$  and (b) Bottleneck-shaped foam samples—showing their 3D pressure drop streamline/arrow plots computed using a superficial fluid inlet velocity of  $10^{-3} \text{ m s}^{-1}$ .

an increase in porous structure permeability. Additionally, structurally eroded RVE samples were also tested for Darcian permeability using similar procedures. With increasing erosion (increasing number of pixels removed), permeability increases due to the reduced structural ligament and lower fluid resistance when compared to “real” samples. Combined permeability data for the “real” and “structural-eroded” samples are plotted in Fig. 6 (to be discussed later), in conjunction with CFD-computed values for inertial-dominated fluids obtained from literature [15, 16].

#### 4. Deep neural network analysis (DNN) of permeability and form drag data

The framework of an artificial neural network (ANN) model requires an understanding of how input ( $x_i$ ) and output signals ( $y_i$ ) are linked by synaptic weights ( $w_i$ ) and biases ( $b_i$ ). According to Fig. 6 (to be discussed later), the fluid-structure and pore-structure-related properties of macroporous materials considered in this study exhibit a power law (non-linear) relationship. Research reported in Ref. [46] found that functions that are not linearly separable result in poor prediction of output signals or expected values using only a single-layer neural network (SNN). Hence, extra-hidden layers (additional neurons) are added to train the neural network to handle this nonlinear relationship

between the input and output signals as shown in Fig. 5. Apart from improving the DNN’s convolution and non-linearity by adding hidden neurons, both input and output signals are set up to be dimensionless and to range between 0 and 1 [37]. Thus, the objective is to sort through the data of permeability and Form drag and to train continuously until predicted output signals match real values as closely as possible.

As shown by Fig. 5, outputs 5 (Darcy permeability [ $k_D$ ]), 6 (Forchheimer permeability [ $k_F$ ]) and 7 (Forchheimer coefficient [ $C_F$ ]) have similar number of inputs and hidden neurons. In order to study outputs 6 and 7, the neural network mathematical functions derived for output 5 can also be used. Ten synaptic weights ( $w_1 - w_{10}$ ) and five biases ( $b_1 - b_5$ ) connect these outputs, hidden signals, and input signals as illustrated by Fig. 5. Hence, the mathematical derivation of the deep neural network which shows the relationship between the output 5, hidden neurons (3 and 4), and input neurons (1 and 2) is therefore derived from the general artificial neural network models [46–48] as presented in the supplementary data. Fig. 6 plots the original (“real”) and DNN predictive reduced permeability and Forchheimer coefficients against material porosity for both the combined TKS and BT-AF foam structures. Fig. 6a-c shows direct exponential relationships between permeability and porosity of the materials, whereas Fig. 6d shows an inverse exponential relationship between Forchheimer coefficient ( $C_F$ ) and material porosity ( $\epsilon$ ). At the beginning of the training, the arbitrarily chosen

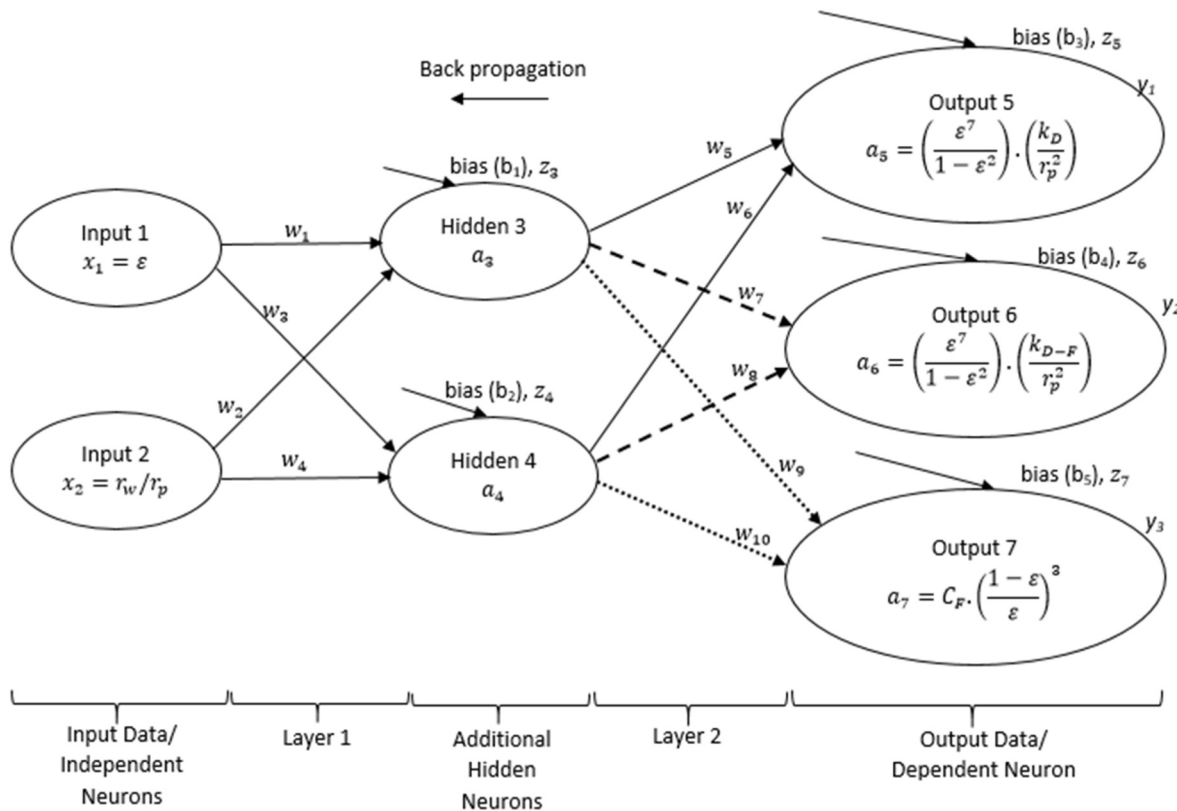


Fig. 5. A schematic representation of deep neural network showing input, additional-hidden and output neurons.

constants were all equal to 1 along with a linearity rate ( $k_L$ ) of 5.0. With increasing material porosity, the output-reduced Darcian permeability values remain unchanged, yielding an overall cost function ( $\sum C$ ) of 0.247 (Fig. 6a).

Training the DNN model in Fig. 5 was accomplished through the use of visual basic for applications (VBA) within Microsoft Excel Spreadsheet. Initially, this step was set up to take 1 s, but was later shortened, resulting in thousands of arbitrary constants resolved achieved within a minute. Additionally, the linearity rate ( $k_L$ ) was changed to ensure accurate and quick convergence of the DNN model. Midway through the calculation, significant changes to the arbitrarily synaptic weights and biases are obtained, leading to a cost function of 0.103 as the DNN predicted data gets closer to the original outputs. Following training with a linearity rate of 10, the cost function for Darcian permeability prediction was reduced to 0.0022 as shown in Table 2. For all foam structures, this reduced cost function of 0.0022 yields predicted values of reduced Darcian permeability that completely overlap the original values. The DNN predicted reduced inertial-dominated permeability values for TKD and BT-AF foams also showed a similar pattern with a correlation near unity (to be discussed later). Furthermore, the permeability values for the BT-AF foams were higher than those for TKD foams, and may be attributed to the higher mean pore openings in the BT-AF foams. Consequently, macroporous materials' pore openings are considered crucial in estimating their permeability [49,50]. Fig. 6c plots reduced Darcy and inertial permeability against porosity for all foam samples. At higher porosities, typically beyond 0.75, inertial-dominated permeability values were slightly elevated than those computed during the Darcy regime of flowing fluid across the interstices of porous materials. The reason could be that at higher gas velocity, the moving fluid permeates the interstices of the macroporous material, traversing pores, openings, and ligaments, leading to more fluid-pore wall contact.

In Table 2, the reduced cost function for inertial-dominated permeability is 0.0031 with a linearity rate of 10, resulting in overlapping output signals from the DNN trained model and the original. As

shown in Fig. 6d, the DNN predicted values for the Forchheimer coefficient decrease exponentially with increasing values of pore volume. The DNN modelling framework resulted in changes of synaptic weights and biases up to a million times within a few weeks after training at a linearity rate of 10. According to Panneerselvam [51], changes in bias during DNN training increase the flexibility of the datasets. As shown in Fig. 5, however, how the material's mean openings and porosity contribute to the framework's predicted output signal is explained by the synaptic weights connecting input signals to hidden neurons. For instance, input 1 ( $x_1 = \varepsilon$ ) is connected to the hidden neurons 3 and 4 via synaptic weights  $w_1$  and  $w_3$  respectively. Similarly, input 2 ( $x_2 = r_w/r_p$ ) is connected to the hidden neurons 3 and 4 by synaptic weights  $w_2$  and  $w_4$  respectively. According to Table 2, at Darcy regime estimations of permeability values for these materials, the reduced mean pore openings linking weight ( $w_2 = 1.593$ ) is higher than the porosity coupling weight ( $w_1 = -9.222$ ). Furthermore, the reduced mean pore openings linking weight ( $w_4 = -4.269$ ) of hidden neuron 4 was much higher than the porosity linking weight ( $w_3 = -13.612$ ). Table 2 shows similar trends for the inertial-dominated reduced permeability values from DNN training. Porosity linking synaptic weights, however, were higher than reduced pore opening linking weights when Forchheimer coefficients were estimated. These, therefore, further reinforce the conclusion given in Refs. [10,11,22,49,50] that pore connectivity greatly governs permeability, whereas porosity significantly affects Forchheimer coefficients for fast-moving fluids.

## 5. Deep neural network analysis (DNN) of effective thermal conductivity data

Using the general artificial neural networks analysis expressed in Eqns 3.0–3.2 (supplementary data), and replacing the terms  $w_5$ ,  $w_6$ ,  $a_5$ ,  $y$ ,  $z_5$  and  $b_3$  in Fig. 5 with  $w_{11}$ ,  $w_{12}$ ,  $a_8$ ,  $y_4$ ,  $z_8$  and  $b_8 = (k_{eff}/k_s)$ , respectively, the new mathematical models for the sum weight, activation and cost function are also presented in the supplementary data.

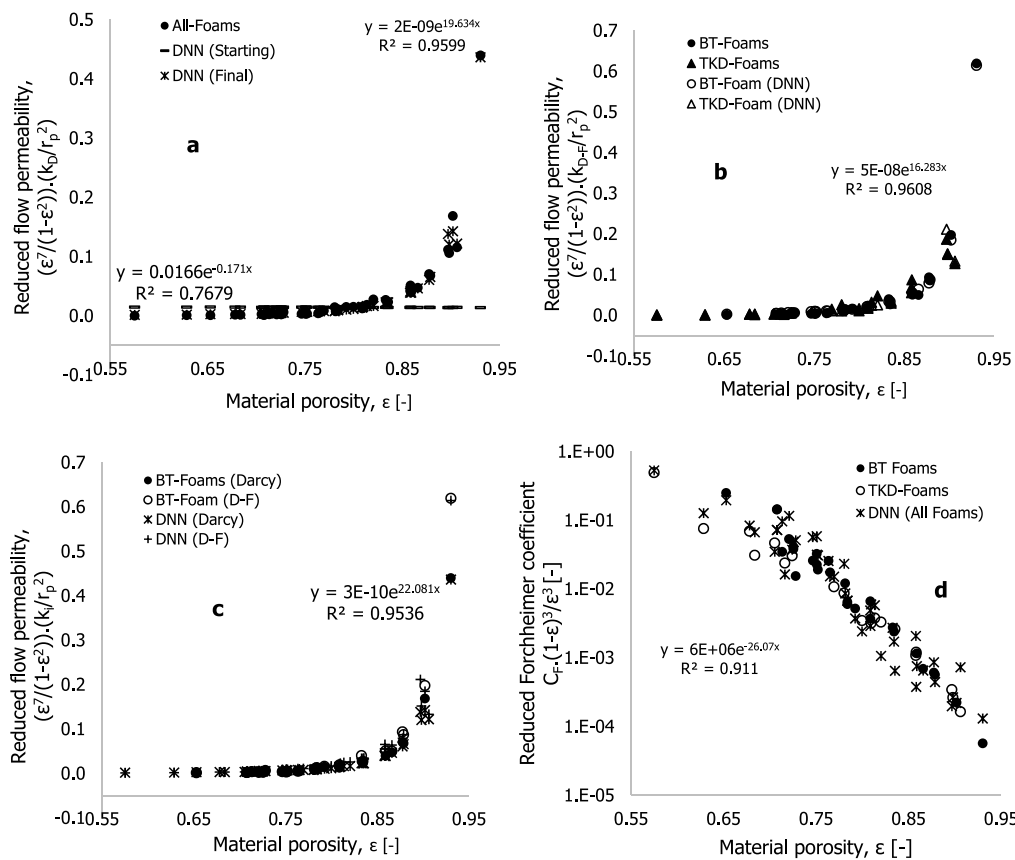


**Fig. 6.** Plots of CFD and DNN predicted data of dimensionless reduced permeability against material porosity for the samples of porous metallic materials for (a) Darcy regime flow (b) Inertial-Dominated (D-F) flow regime (c) Darcy and D-F flow regimes and (d) reduced Forchheimer coefficient against material porosity.

**Fig. 7** compares the DEM/CFD (“real”) and DNN predictions of normalised effective thermal conductivity ( $k_{eff}/k_s$ ) against material porosity ( $\epsilon$ ) for solid materials (Al, Concrete, Alumina and Al3003 – H18), assuming water and air as interstitial fluids. It is important to note that both solid and fluid properties are chosen to represent their inherent properties using similar RVE foam–fluid systems. **Table 3** summarizes the synaptic weights, biases, linearity rates, and cost functions of the DNN trained data for all foam–fluid systems. **Fig. 7** shows that the normalised effective thermal conductivity of macroporous foam–fluid systems is inversely (logarithmically) related to material porosity. With initial values of 1.0 for all weights and biases and a linearity rate of 10, values for the normalised effective thermal conductivity remain unchanged with increasing values of material porosity, as shown in **Fig. 7a**. These initial guess values yielded a cost function of 4.381, which then decreased to 2.01 and then to 0.0055 after multiple training runs, resulting in significant changes in the estimated values for synaptic weights and final biases. The final values of the trained/predicted DNN output signal of the normalised effective thermal conductivity, which reduces the cost function to 0.0055, closely match the “real” output signal used during training.

**Fig. 7b** presents plots of the “real” and DNN predicted data of  $k_{eff}/k_s$  against  $\epsilon$  for Concrete–Air and Concrete–Water foam–fluid systems. The Concrete–Water foam–fluid system was observed to have higher values of  $k_{eff}/k_s$  than the Concrete–Air system which is likely due to the higher thermal conductivity of the water ( $k_{H_2O} = 0.6 \text{ W.m}^{-1.K}^{-1}$ ) over air ( $k_{Air} = 0.024 \text{ W.m}^{-1.K}^{-1}$ ). Additionally, **Fig. 7c** also shows that the Al–Water and Alumina–Water systems contribute more to the effective thermal conductivity of foam–fluid systems when compared to air as the interstitial fluid. A slight increase in water contribution to  $k_{eff}/k_s$  for

foam–fluid systems can be seen in **Fig. 7c** as compared with the much wider variations for Concrete–Fluid systems in **Fig. 7b**. This may largely be the result of the higher thermal conductivity of Al ( $k_{Al} = 238 \text{ W.m}^{-1.K}^{-1}$ ), Alumina ( $k_{Al_2O_3} = 27 \text{ W.m}^{-1.K}^{-1}$ ) and Al3003–H18 ( $k_{Al3003-H18} = 155 \text{ W.m}^{-1.K}^{-1}$ ) foams in comparison to the concrete foams ( $k_{Concrete} = 1.8 \text{ W.m}^{-1.K}^{-1}$ ). This indicates that both the thermal conductivity of the solid matrixes and that of the fluid play a critical role in the estimation of the normalised effective thermal conductivity for foam–fluid systems. According to experimental, theoretical and numerical simulation data obtained in Refs. [28–35], the effective thermal conductivity of macroporous foam–fluid systems increases as the solid content’s thermal conductivity increases. When keeping the interstitial fluid constant, it is expected that the effective thermal conductivity of most porous metallic–fluid systems will be higher than that of other solid matrixes (like polymer, wood, fibrous, concrete, bones, etc.).

**Fig. 8** further illustrates how water dominates air as an interstitial fluid using the DNN predicted output data. This figure illustrates the nonlinear (direct exponential) relationship between water’s percentage contribution over air as a function of increasing porosity. These values are significantly higher for concrete foams than for aluminum foams. This shows the role water plays as an interstitial fluid in estimating the normalised effective thermal conductivity of foam–fluid systems is augmented for macroporous materials characterized by low thermal conductivity but decreases as the solid thermal conductivity increases. With increasing structure porosity, the contribution of water to the Concrete–Fluid system increases the normalised effective thermal conductivity up to 9 times, whereas the Al–Fluid system’s contribution only increases from 0.18 to 37.50. Alumina–Fluid and Al3003–H18–Fluid systems showed similar direct exponential trends in water contribution

**Table 2**

Tabular representation of proposed DNN models for permeability and Form drag of porous metallic structures.

	DNN Models	Optimized arbitrary constants	$k_L$	$\sum C$
Darcian permeability, $k_D$ [m <sup>2</sup> ]	$\left(\frac{\varepsilon^7}{1-\varepsilon^2}\right) \cdot \left(\frac{k_D}{r_p^2}\right) = \frac{1}{1+e^{-Z_5}}$ $Z_5 = b_3 + \frac{w_5}{1+e^{-Z_5}} + \frac{w_6}{1+e^{-Z_4}}$ $Z_3 = b_1 + w_1 \cdot \varepsilon + w_2$ $r_w/r_p$ $Z_4 = b_2 + w_3 \cdot \varepsilon + w_4 \cdot r_w/r_p$	$b_1 = 7.557$ $w_1 = -9.222$ $w_2 = 1.593$ $b_2 = 16.506$ $w_3 = -13.612$ $w_4 = -4.270$ $b_3 = 13.047$ $w_5 = -7.056$ $w_6 = -12.779$	10	0.0022
Inertial-dominated permeability, $k_i$ [m <sup>2</sup> ]	$\left(\frac{\varepsilon^7}{1-\varepsilon^2}\right) \cdot \left(\frac{k_i}{r_p^2}\right) = \frac{1}{1+e^{-Z_6}}$ $Z_6 = b_4 + \frac{w_7}{1+e^{-Z_5}} + \frac{w_8}{1+e^{-Z_4}}$ $Z_3 = b_1 + w_1 \cdot \varepsilon + w_2$ $r_w/r_p$ $Z_4 = b_2 + w_3 \cdot \varepsilon + w_4 \cdot r_w/r_p$	$b_1 = 7.427$ $w_1 = -9.596$ $w_2 = 1.256$ $b_2 = 19.824$ $w_3 = -13.805$ $w_4 = -9.015$ $b_4 = 14.319$ $w_7 = -7.596$ $w_8 = -14.119$	10	0.0031
Forchheimer coefficient, $C_F$ [m <sup>2</sup> ]	$C_F \cdot \left(\frac{1-\varepsilon}{\varepsilon}\right)^3 = \frac{1}{1+e^{-Z_7}}$ $Z_7 = b_5 + \frac{w_9}{1+e^{-Z_5}} + \frac{w_{10}}{1+e^{-Z_4}}$ $Z_3 = b_1 + w_1 \cdot \varepsilon + w_2$ $r_w/r_p$ $Z_4 = b_2 + w_3 \cdot \varepsilon + w_4 \cdot r_w/r_p$	$b_1 = -8.358$ $w_1 = 8.019$ $w_2 = 5.007$ $b_2 = -1.356$ $w_3 = -33.351$ $w_4 = 44.731$ $b_5 = -0.117$ $w_9 = -9.992$ $w_{10} = 19.956$	5	0.032

values, ranging from 8.65 to 203.06 and 1.52 to 54.20 respectively.

**Table 3** also presents the final DNN modelling equivalence (Eqns 4.4 and 4.5) for estimating the normalised effective thermal conductivity of macroporous foam–fluid systems along with their estimated trained values of synaptic weights ( $w_i$ ), biases ( $b_i$ ), linearity rates ( $k_L$ ) and reduced cost functions ( $\sum C$ ). For the macroporous foam–fluid systems, the reduced cost functions were found to range between 0.0055 and 0.204 with a constant linearity rate of 10. Material porosity has traditionally been considered the pore–structure–related property of macroporous structures that solely defines their effective thermal conductivity [12,18,30,52–54]. According to Otaru et al. [29], porosity plays the dominant role in estimating the effective thermal conductivity of macroporous foam–fluid systems, with other pore–structure–related parameters playing a secondary role. By analyzing the final DNN modelled synaptic weights ( $w_1 – w_4$ ) linking the inputs to the hidden nodes (3 and 4), the extent to which pore–structure related parameters contribute to the effective thermal conductivity of these foam–fluid systems can be better explained. Based on **Table 3**, input 2 (reduced mean pore openings) contributed between 5.8 and 13.2 percentage points, which is much lower than the contribution of materials’ porosity (input 1). In comparison, the reduced mean pore openings ( $r_w/r_p$ ) appeared to play a greater role for the Al–Water system and a lesser role for the Concrete–Air system, the foam–fluid systems estimated to have the highest and lowest effective thermal conductivity, respectively.

The application of artificial intelligence’s machine learning backpropagation technique has so far resulted in the formulation of mathematical models for predicting macroporous foam – fluid permeability, Forchheimer coefficient, and effective thermal conductivity. This study used CFD data as the basis for learning machine learning models, and

these data have been substantiated in the literature as shown in **Fig. 2**. Acquisition of CFD data is challenging due to factors such as high computational demand and time. The high computational demand results from the pore-scale approach used for the CFD data acquisition - using high-resolution images, workable representative volume elements and optimized mesh structures to accurately describe velocity and pressure gradients of foam–fluid structures. These machine learning DNN formulated models may be used to estimate the three variables (permeability, Forchheimer coefficient, and effective thermal conductivity) for a macroporous foam–fluid system, however it is imperative that the confidence of the formulated models be substantiated in the future to predict similar macroporous materials and design them. Correlations between numerically simulated CFD and DNN calculated data for (a) permeability at Darcy and Darcy–Forchheimer flow regimes, (b) Forchheimer coefficient, and (c) effective thermal conductivity are shown in **Fig. 9**. All variables showed direct linear relationships and estimated correlation coefficients greater than 90%. For both Al–Air and Al–Water macroporous foam–fluid systems, approximately 91% for the Darcy and Darcy–Forchheimer permeability values, 93% for the Forchheimer coefficient, and more than 98 % for the normalised effective thermal conductivities. Nevertheless, it is noteworthy to recognize that the DNN framework can be continuously trained until its overall cost function reaches zero thereby closing the gap between the estimated correlation coefficients and a maximum of 100 %. In the current study, the framework in **Fig. 5** was continuously and rigorously trained for approximately two months along with mathematical models formulated by DNN. According to past and current experience from this study, additional training of six months would be needed to improve the correlation coefficients between permeability and Forchheimer coefficients to close to 100% and to substantially reduce the cost function (**Table 2**). Convolution and non-linearity between input and output datasets are the main reasons for the anticipated increase in computational time for the simulation of synaptic weights and biases needed to predict future events.

## 6. Conclusion

In this study, a machine learning backpropagation network analysis is used to train and develop models for estimating macroporous structure Darcian permeability, Darcy–Forchheimer permeability, Forchheimer coefficient, and effective thermal conductivity. In addition, Darcy permeability values for slow–moving fluids across materials’ representative interstices were determined by combining three-dimensional advanced imaging with computational fluid dynamics (CFD) modelling and simulation. Based on the range of material porosity considered herein, Forchheimer permeability was consistently higher than Darcian permeability. Additionally, facsimile representations of foam–fluid systems were acquired through imaging, to provide additional heat and flow datasets needed for a robust machine learning application. Through machine learning deep neural networks, permeability, Forchheimer coefficient and effective thermal conductivity of foam–fluid systems are linked to input signals via several synaptic weights and biases, resulting in predictions that were more than 90% correlated with CFD results. Interstitial fluid (water and air) and pore–structure–related information for these macroporous materials were also evaluated for any causative role. While material porosity ( $\varepsilon$ ) was observed to play a dominant role in determining Forchheimer coefficient and effective thermal conductivity, reduced mean pore openings ( $r_w/r_p$ ) of the structures were also observed to be crucial towards accurate estimation of their permeability. Consequently, the trained DNN predicted data support findings given in Refs. [28–36] that material porosity greatly influences the effective thermal conductivity and Forchheimer coefficient of macroporous foam–fluid systems. For the range of structures considered in this study, the reduced mean pore openings were found to be between 5.8 and 13.2%.

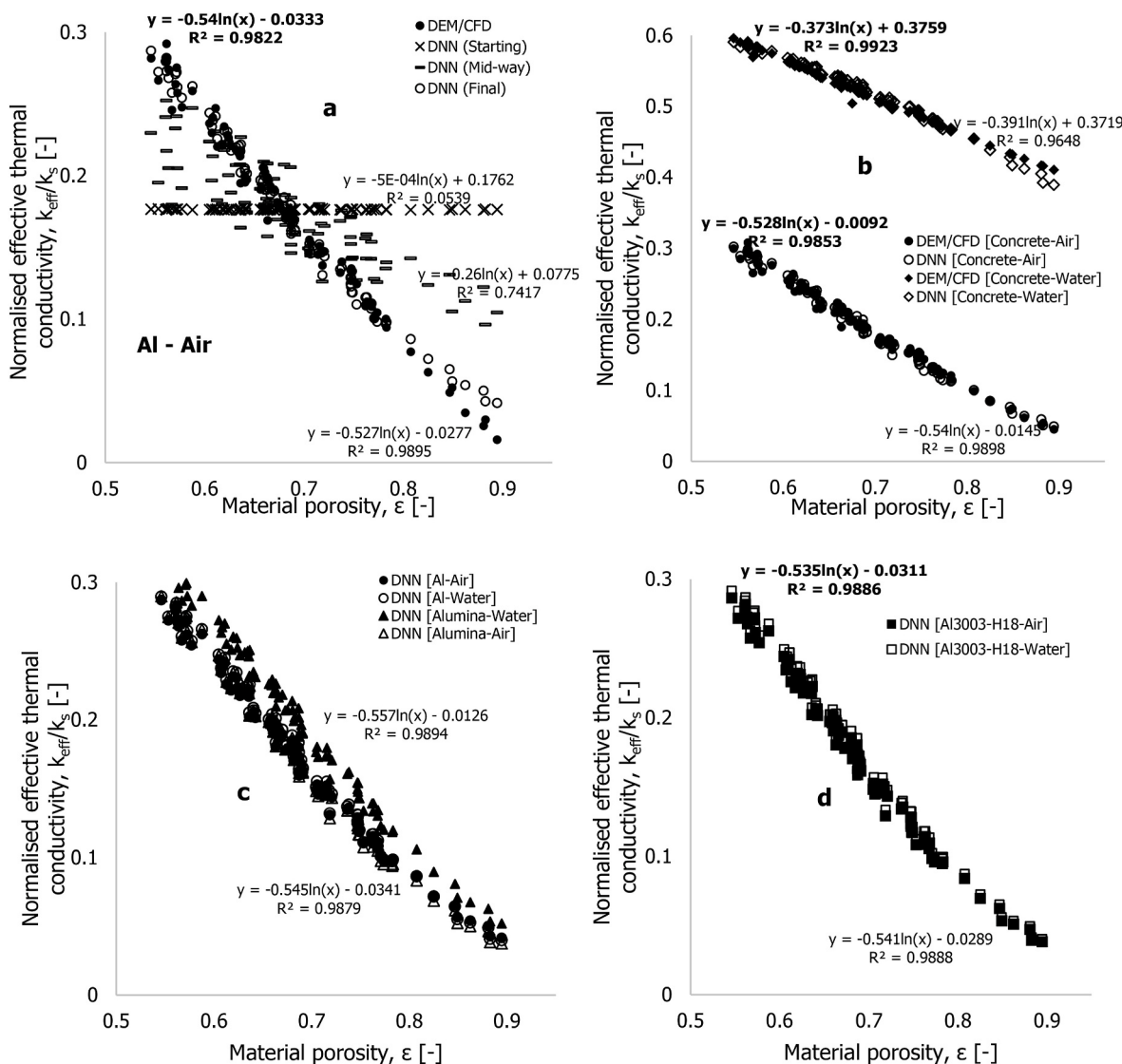


**Fig. 7.** Plots of DEM/CFD and DNN computed values of normalised effective thermal conductivity,  $k_{eff}/k_s$  [-] against material porosity,  $\epsilon$  [-] for different kind of foam-fluid systems.

**Table 3**

Tabular representation of trained DNN data for the prediction of the normalised effective thermal conductivity ( $k_{eff}/k_s$ ) of different class of foam-fluid systems.

Foam-fluid	$b_1$	$w_1$	$w_2$	$b_2$	$w_3$	$w_4$	$b_3$	$w_5$	$w_6$	$k_L$	$\sum C$	% of $r_w/r_p$
Al-Air	-4.585	4.359	0.428	-3.193	2.828	0.224	0.294	-5.308	-3.851	10	0.0055	7.9-8.9
Al-Water	-4.888	4.625	0.514	-3.363	2.889	0.191	0.191	-5.491	-3.907	10	0.0106	6.6-10.0
Concrete-Air	-4.957	4.575	0.476	-3.393	2.859	0.165	0.181	-5.480	-3.897	10	0.0118	5.8-9.4
Concrete-Water	-4.955	4.578	0.478	-3.343	2.950	0.242	0.986	-0.096	-3.926	10	0.2040	8.2-9.5
Alumina-Air	-4.884	4.666	0.532	-3.370	2.904	0.199	0.210	-5.507	-3.912	10	0.0108	6.9-10.2
Alumina-Water	-4.971	4.584	0.478	-3.411	2.861	0.168	0.221	-5.481	-3.896	10	0.0138	9.4-13.2
Al3003-H18-Air	-4.911	4.660	0.517	-3.374	2.906	0.192	0.176	-5.509	-3.915	10	0.0107	6.6-10.0
Al3003-H18-Water	-4.923	4.653	0.514	-3.382	2.900	0.190	0.188	-5.507	-3.912	10	0.0107	6.6-10.0

Final Equation.

$$\frac{k_{eff}}{k_s} = \frac{1}{(1 + e^{-z_8})} \text{ and } z_8 = b_6 + \frac{w_{11}}{1 + e^{-z_3}} + \frac{w_{12}}{1 + e^{-z_4}} \text{ Eqn 4.4.}$$

$$z_3 = b_1 + w_1 \cdot \epsilon + w_2 \cdot r_w/r_p \text{ and } z_4 = b_2 + w_3 \cdot \epsilon + w_4 \cdot r_w/r_p \text{ Eqn 4.5.}$$

#### CRediT authorship contribution statement

**Abdulrazak Jinadu Otaru:** Conceptualization, Data curation, Formal analysis, Investigation, Methodology, Project administration, Resources, Software, Validation, Visualization, Writing – original draft.

**Manase Auta:** Formal analysis, Project administration, Writing – review & editing.

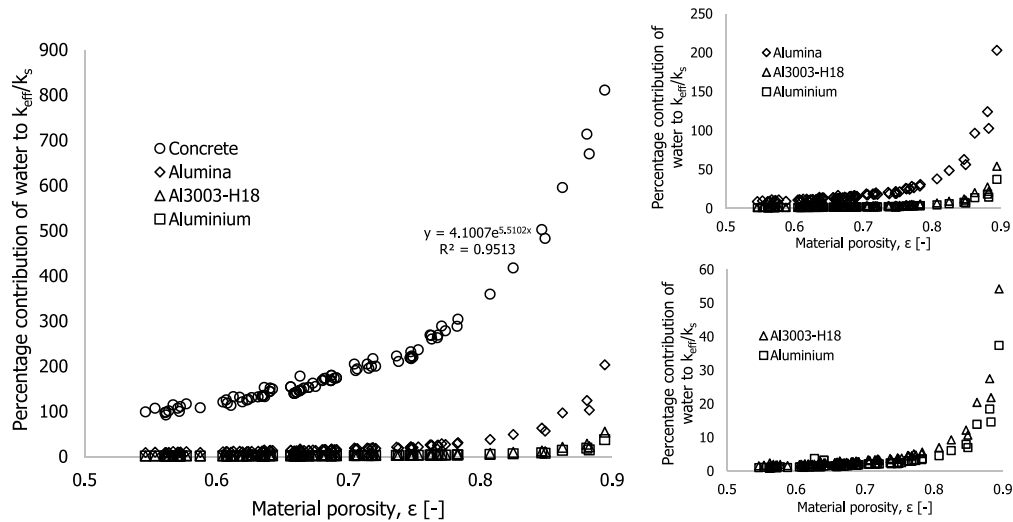


**Fig. 8.** Plots of DNN computed percentage contribution of water (over air) on the normalised effective thermal conductivity of foam-fluid systems against material porosity,  $\epsilon$  [-].

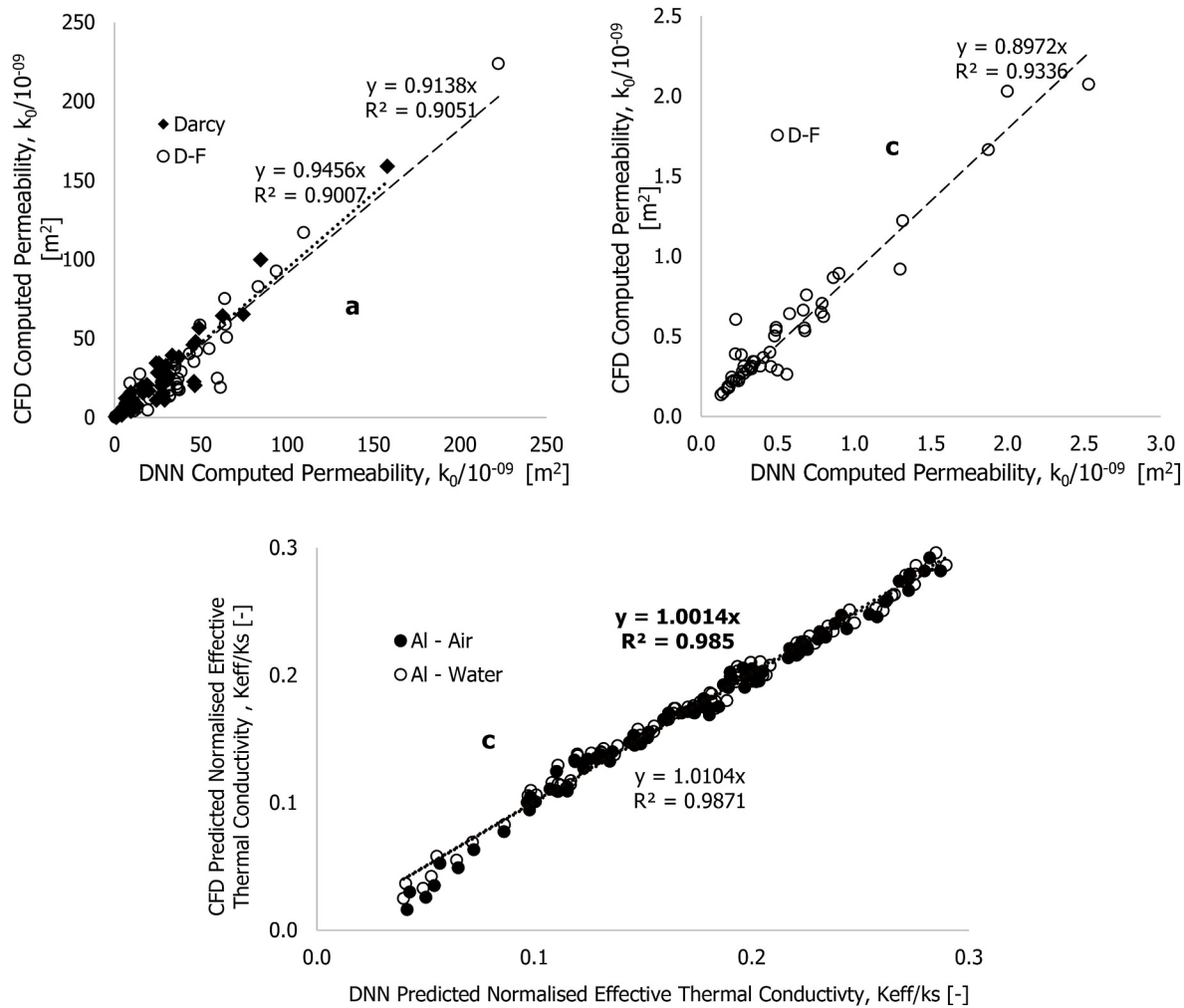


**Fig. 9.** Plots of CFD numerically simulated against DNN predicted values of (a) Darcy and Darcy-Forchheimer permeability, (b) Forchheimer coefficient and (b) normalised effective thermal conductivity obtained for the macroporous-foam fluid systems.

## Declaration of competing interest

The authors declare that they have no known competing financial interests or personal relationships that could have appeared to influence the work reported in this paper.

## Data availability

Data will be made available on request.

## Acknowledgement

Licenses and technical support provided by Synopsys-Simpleware and Bowers and Wilkins (B & W) Group are particularly appreciated. Thanks to King Faisal University for providing a conducive study environment for Dr. AJ.

## Appendix A. Supplementary data

Supplementary data to this article can be found online at <https://doi.org/10.1016/j.ijthermalsci.2024.109039>.

## References

- [1] H. Darcy, *Les Fontaines Publiques de la Ville de Dijon*, Dalmont, Paris, 1856.
- [2] A. Bhattacharya, V.V. Calmidi, R.L. Mahajan, Thermophysical properties of high porosity metal foams, *Int. J. Heat Mass Tran.* 45 (2002) 1017–1031.
- [3] J.M. Coulson, The flow of fluids through granular beds: effects of particle shape and voids in streamline flow, *Trans. Inst. Chem. Eng.* 27 (1949) 237–257.
- [4] S. Ergun, Fluid flow through packed columns, *Chem. Eng. Prog.* 48 (1952) 89–94.
- [5] P.C. Carman, Fluid flow through granular beads, in: *Chemical Engineering Research & Design vol. 15, Transactions of the Institution of Chemical Engineers Part A*, 1937, pp. 415–421.
- [6] D.A. Nield, A. Bejan, *Convection in Porous Media*, second ed., Springer, New York, 1992, pp. 8–91.
- [7] F.A.L. Dullien, *Porous Media: Fluid Transport and Pore Structure*, Academic Press, New York, 1979.
- [8] A.J. Otaru, A.R. Kennedy, Investigation of the pressure drop across packed beds of spherical beads: comparison of empirical models with pore-level computational fluid dynamics simulations, *ASME Fluids Eng'g.* 141 (2019), 071305-1.
- [9] N. Dukhan, Correlations for the pressure drop for flow through metal foam, *Exp. Fluid* 41 (2006) 665–672.
- [10] J.F. Liu, W.T. Wu, W.C. Chiu, W.H. Hsieh, Measurement and correlation of friction characteristic of flow through foam matrices, *Exp. Therm. Fluid Sci.* 30 (2006) 329–336.
- [11] A.J. Otaru, M.B. Samuel, Pore-level CFD investigation of velocity and pressure dispositions in microcellular structures, *Mater. Res. Express* 8 (2021) 046516.
- [12] J.W. Paek, B.H. Kang, S.Y. Kim, J.M. Hyun, Effective thermal conductivity and permeability of aluminium foam materials, *Int. J. Thermophys.* 21 (2) (2000) 453–464.
- [13] N. Dukhan, *Metal Foams: Fundamental and Applications*, DESTECH Publication, Inc. Technology & Engineering, USA, 2013, pp. 1–310.
- [14] H. Yang, Y. Li, B. Ma, Y. Zhu, Review and a theoretical approach on pressure drop correlations of flow through open-cell metal foams, *Materials* 14 (2021) 3153.
- [15] A.J. Otaru, H.P. Morvan, A.R. Kennedy, Measurement and simulation of pressure drop across replicated microcellular aluminium in the Darcy-forchheimer regime, *Acta Mater.* 149 (2018) 265–275.
- [16] A.J. Otaru, M. Abdulkadir, M.R. Corfield, A. Kenfack, N. Tanko, Computational evaluation of effective transport properties of differential microcellular structures, *AIChE J.* (2020) e16928, <https://doi.org/10.1002/aic.16928>.
- [17] K. Boomsma, D. Poulikakos, F. Zwick, Metal foams as compact high performance heat exchangers, *Mech. Mater.* 35 (2003) 1161–1176.
- [18] S. Mahjoob, K. Vafai, A synthesis of fluid and thermal transport models for metal foam heat exchanger, *Int. J. Heat Mass Tran.* 5 (2008) 3701–3711.
- [19] A. Bhattacharya, R.L. Mahajan, Finned metal foam heat sinks for electronics cooling in forced convection, *J. Electron. Packag.* 124 (2002) 155–163.
- [20] Y. Wang, K. Vafai, An experimental investigation of the thermal performance of an asymmetrical flat heat pipe, *Int. J. Heat Mass Tran.* 43 (2000) 2657–2668.
- [21] A. Dybbs, R.V. Edwards, A New Look at Porous Media Fluid Mechanics-Darcy to Turbulent, in: J. Bear, M.Y. Nato ASI series E, 1984.
- [22] D. Edouard, M. Lacroix, C.P. Huu, F. Luck, Pressure drop modelling on solid foam: state-of-the-art correlation, *Chem. Eng. J.* 144 (2008) 299–311.
- [23] A.J. Otaru, A.R. Kennedy, The permeability of virtual macroporous structures generated by sphere-packing models: comparison with analytical models, *Scripta Mater.* 124 (2016) 30–33.
- [24] L. Weber, D. Ingram, S. Guardia, A. Athanasiou-Ioannou, A. Mortensen, Fluid flow through replicated microcellular materials in the Darcy-forchheimer regime, *Acta Mater.* 126 (2017) 280–293.
- [25] V.V. Calmidi, R.L. Mahajan, The effective thermal conductivity of high porosity fibrous metal foams, *ASME J. Heat Transfer* 121 (1999) 466–471.
- [26] Ö. Bağcı, N. Dukhan, Experimental hydrodynamics of high – porosity metal foam: effect of pore density, *Int. J. Heat Mass Tran.* 103 (2016) 879–885.
- [27] A.J. Otaru, M.S. Muhammad, M.B. Samuel, A.G. Olugbenga, M.E. Gana, M. R. Corfield, Pressure drop in high-density porous metals via tomography datasets, accepted for publication in met, *Mater. Int.* (2019), <https://doi.org/10.1007/s12540-019-00431-y>.
- [28] A.J. Otaru, M. Abdulkadir, A.S. Kovo, M.R. Corfield, N. Tanko, O.A. Odey, A. Kenfack, U.O. Aroke, Three-dimensional high-resolution image inversion and pore level CFD characterisation of effective thermal conductivity of replicated microcellular structures, *Int. J. Thermofluids* 14 (2022) 100141.
- [29] A.J. Otaru, R.O. Isa, A.U. Emene, A.A. Faruq, P.O. Sedemogun, S.M. Hassan, The effective thermal conductivity of virtual macroporous structures, *Results Eng.* 15 (2022) 100531.
- [30] A.F. Abuserwal, E.M.E. Luna, R. Goodall, R. Woolley, The effective thermal conductivity of open cell replicated aluminium metal sponges, *Int. J. Heat Mass Tran.* 108 (B) (2017) 1439–1448.
- [31] E. Solorzano, J.A. Reglero, M.A. Rodriguez-Perez, D. Lehmbus, M. Wichman, J. A. de Saja, An experimental study on the thermal conductivity of aluminium foams by using the transient plane source method, *Int. J. Heat Mass Tran.* 51 (2008) 6259–6267.
- [32] X.H. Yang, J.J. Kuang, T.J. Lu, F.S. Han, T. Kim, A simplistic analytical unit cell based model for the effective thermal conductivity of high porosity open-cell metal foams, *J. Phys. D* 46 (2013) 255302.
- [33] K. Boomsma, D. Poulikakos, On the effective thermal conductivity of a three-dimensionally fluid-saturated metal foam, *Int. J. Heat Mass Tran.* 44 (2001) 827–836.
- [34] Z. Dai, K. Nawaz, Y.G. Park, J. Bock, A.M. Jacobi, Correcting and extending the Boomsma-Poulikakos effective thermal conductivity model for three-dimensional, fluid-saturated metal foams, *Int. Commun. Heat Mass Tran.* 37 (2010) 575–580.
- [35] K. Boomsma, D. Poulikakos, Corrigendum for the paper: K. Boomsma, D. Poulikakos, "On the effective thermal conductivity of a three-dimensionally structured fluid-saturated metal foam", *Int. J. Heat Mass Tran.* 44 (2001) 827–836. International Journal of Heat and Mass Transfer, Vol 54, Ppp. 746–748.
- [36] A. Tikadar, S. Kumar, Investigation of thermal hydraulic performance of metal-foam heat sink using machine learning approach, *Int. J. Heat Mass Tran.* 199 (2022) 123438.
- [37] M. Calati, G. Righetti, L. Doretti, C. Zilio, G.A. Longo, K. Hooman, S. Mancin, Water pool boiling in metal foams: from experimental results to a generalised model based on artificial neural network, *Int. J. Heat Mass Tran.* 176 (2021) 121451.
- [38] M. Babanezhad, I. Behroyan, A.T. Nakjiri, A. Marjani, S. Shirazian, Computational modelling of transport in porous media using an adaptive network – based fuzzy inference system, *ACS Omega* 5 (2020) 30826–30835.
- [39] C. Lorreyte, P. Lea, J.-F. Henry, J. Adrien, E. Maire, H. Pron, Morphological and effective thermal transport properties of fixed beds of wood chips: toward realistic modelling of low – temperature pyrolysis, *J. Renew. Sustain. Energy* 12 (1) (2022) 013101.
- [40] H. Oun, A.R. Kennedy, Tailoring the pressure drop in multi-layered open-cell porous Inconel structures, *J. Porous Mater.* 2 (2015) 1627–1633.
- [41] T.P. De Carvalho, H.P. Morvan, D. Hargreaves, H. Oun, A. Kennedy, Pore-Scale Numerical Investigation of Pressure Drop Behaviour across Open-Cell Metal Foams, *Trans Porous Med.* 2017, <https://doi.org/10.1007/s11242-017-0835-y>.
- [42] A.J. Otaru, Unpublished Research, University of Nottingham, 2018.
- [43] A.J. Otaru, H.P. Morvan, A.R. Kennedy, Airflow Measurement across Negatively-Infiltration Processed Porous Aluminium Structures, vol. 65, American Institute of Chemical Engineers AIChE J, 2019, pp. 1355–1364.
- [44] J.L. Lage, P.S. Krueger, A. Narasimhan, Protocol for measuring permeability and form coefficient of porous media, *Phys. Fluids* (2005) 17–88101.
- [45] N. Dukhan, Ö. Bağcı, M. Özdemir, Metal foam hydrodynamics: flow regimes from pre – Darcy to turbulence, *Int. J. Heat Mass Tran.* 77 (2014) 114–123.
- [46] A. Sircar, K. Yadav, K. Rayavarapu, N. Bist, H. Oza, Application of machine learning and artificial intelligence in oil and gas industry, *Petrol. Res.* 6 (2021) 379–391.
- [47] G. Baiocco, V. Tagliaferri, N. Ucciardello, Neural networks implementation for analysis and control of heat exchange process in a metal foam prototypal device, in: 10th CIRP Conference on Intelligent Computation in Manufacturing Engineering – Procedia CIRP, 16, 2017, pp. 518–522.
- [48] A.J. Otaru, Research of the numerical simulation and machine learning backpropagation networks analysis of the sound absorption properties of cellular soundproofing materials, *Results Eng.* 20 (2023) 101588.
- [49] J.F. Despois, A. Mortensen, Permeability of open-pore microcellular materials, *Acta Mater.* 53 (2005) 1381–1388.
- [50] J.F. Despois, A. Marmottant, L. Salvo, A. Mortensen, Influence of the infiltration pressure on the structure and properties of replicated aluminium foams, *Mater. Sci. Eng. A* 462 (2007) 68–75.
- [51] L. Panneerselvam, Activation functions and their derivatives – a quick and complete guide (deep learning). <https://www.analyticsvidhya.com/blog/2021/04/activation-functions-and-their-derivatives-a-quick-complete-guide/>, 2023.

- [52] G.N. Dul'nev, Heat transfer through solid disperse systems, *J. Eng. Phys.* 9 (1965) p275.
- [53] E. Takegoshi, Y. Hirasawa, J. Matsuo, K. Okui, A study on effective thermal conductivity of porous metals, *Trans. Japan Soc. Mech. Engineers B* 58 (547B) (1992) p879.
- [54] X. Xiao, P. Zhang, M. Li, Effective thermal conductivity of open-cell metal foams impregnated with pure paraffin for latent heat storage, *Int. J. Therm. Sci.* 81 (2014) 94–105.